Analysis of biosurfaces by neutron reflectometry: From simple to complex interfaces

Ann Junghans, Erik B. Watkins, Robert D. Barker, Saurabh Singh, Mary Jo Waltman, Hillary L. Smith, Luka Pocivavsek, and Jaroslaw Majewski

Citation: Biointerphases **10**, 019014 (2015); doi: 10.1116/1.4914948
View online: http://dx.doi.org/10.1116/1.4914948
View Table of Contents: http://scitation.aip.org/content/avs/journal/bip/10/1?ver=pdfcov
Published by the AVS: Science & Technology of Materials, Interfaces, and Processing

Analysis of biosurfaces by neutron reflectometry: From simple to complex interfaces

Ann Junghans
MPA-CINT/Lujan Neutron Scattering Center, Los Alamos Neutron Science Center, Los Alamos National Laboratory, Los Alamos, New Mexico 87545

Erik B. Watkins
MPA-11/Lujan Neutron Scattering Center, Los Alamos Neutron Science Center, Los Alamos National Laboratory, Los Alamos, New Mexico 87545 and Institut Laue Langevin, 71 Avenue des Martyrs, CS 20156, 38042 Grenoble Cedex 9, France

Robert D. Barker
Institut Laue Langevin, 71 Avenue des Martyrs, CS 20156, 38042 Grenoble Cedex 9, France

Saurabh Singh
MPA-CINT/Lujan Neutron Scattering Center, Los Alamos Neutron Science Center, Los Alamos National Laboratory, Los Alamos, New Mexico 87545

Mary Jo Waltman
Biosciences Division, Bioenergy and Biome Sciences, Los Alamos National Laboratory, Los Alamos, New Mexico 87545

Hillary L. Smith
Department of Applied Physics and Materials Science, California Institute of Technology, Pasadena, California 91125

Luka Pocivavsek
Department of Surgery, University of Pittsburgh Medical Center, Pittsburgh, Pennsylvania 15213

Jaroslaw Majewski[a)]
MPA-CINT/Lujan Neutron Scattering Center, Los Alamos Neutron Science Center, Los Alamos National Laboratory, Los Alamos, New Mexico 87545

(Received 15 December 2014; accepted 5 February 2015; published 16 March 2015)

Because of its high sensitivity for light elements and the scattering contrast manipulation via isotopic substitutions, neutron reflectometry (NR) is an excellent tool for studying the structure of soft-condensed material. These materials include model biophysical systems as well as *in situ* living tissue at the solid–liquid interface. The penetrability of neutrons makes NR suitable for probing thin films with thicknesses of 5–5000 Å at various buried, for example, solid–liquid, interfaces [J. Daillant and A. Gibaud, Lect. Notes Phys. **770**, 133 (2009); G. Fragneto-Cusani, J. Phys.: Condens. Matter **13**, 4973 (2001); J. Penfold, Curr. Opin. Colloid Interface Sci. **7**, 139 (2002)]. Over the past two decades, NR has evolved to become a key tool in the characterization of biological and biomimetic thin films. In the current report, the authors would like to highlight some of our recent accomplishments in utilizing NR to study highly complex systems, including *in-situ* experiments. Such studies will result in a much better understanding of complex biological problems, have significant medical impact by suggesting innovative treatment, and advance the development of highly functionalized biomimetic materials. © *2015 American Vacuum Society*. [http://dx.doi.org/10.1116/1.4914948]

I. INTRODUCTION

Understanding biological systems on a nanometer-resolution scale[1–3] is important for solving complex biological problems, develop innovative treatment, and advance the development of highly functionalized biomimetic materials. A multitude of techniques exist for studying biorelated systems of various complexity, such as interference reflection microscopy,[4–8] fluorescence interference contrast microscopy,[9–11] total internal reflection fluorescence microscopy,[12–16] surface plasmon resonance microscopy,[17,18] transendothelial electrical resistance,[19–22] atomic force microscopy (AFM),[23–26] electrical impedance spectroscopy,[27–29] and numerous more.

Over the past decades, neutron reflectometry (NR) has become a key tool in the characterization of biological and biomimetic thin films.[2,30] Typically, NR measurements are performed on homogeneous model systems, such as phospholipid monolayers at the air–liquid interface,[31] pure and hybrid phospholipid bilayers on silicon and quartz substrates,[32–35] and supported phospholipid bilayers mimicking biological membranes.[36–38] For more information, we refer the interested reader to several recent reviews and publications.[3,30,39–42] Small angle neutron scattering is also frequently employed to study living matter. One of the many recent examples are studies of suspensions of actively

[a)]Electronic mail: jarek@lanl.gov

metabolizing human erythrocytes and thermal fluctuations of hemoglobin.[43,44] In the current paper, we would like to highlight recent advances in utilizing neutron scattering to study biorelated structure in dynamic conditions (under the shear flow) including *in-situ* investigations of the interfacial properties of living cells. NR can be applied in the study of living tissue to better understand biological mechanisms such as cellular adhesion within the vascular system and the differences that may be specifically associated with brain tumor invasion.[45–47]

II. METHOD

NR is an excellent tool for studying the structure of biological molecules and living tissue at the solid–liquid interface *in situ*. Due to the penetrability of neutrons, NR is commonly used to probe thin films with thicknesses of 5–5000 Å at buried solid–liquid interfaces. Neutrons are highly sensitive to the scattering contrast between hydrogenated and deuterated materials. An example is neutron scattering from hydrogenated alkyl tails of phospholipid bilayers (which are not capable of an isotopic exchange with the solvent) measured in a deuterated subphase (D_2O). During a NR experiment, neutrons penetrate through the support substrate (e.g., quartz wafer), which is in contact with the liquid subphase. The roughness and nature of this substrate is crucial for the measurements.[48–51] The neutrons are scattered from the structure of interest, for example, living cells deposited on the substrate, at a small angle, θ [Fig. 1(b)]. In NR, the ratio of elastically and specularly scattered neutrons to incident neutrons is measured. This ratio is defined as the reflectivity, R, and is measured as a function of the momentum transfer vector, Q_z, where $Q_z = 4\pi \sin[\theta]\lambda^{-1}$ and λ is the neutron wavelength. For monochromatic neutron beams, frequently employed at nuclear reactor source, the variation in the magnitude of Q_z vector is achieved via changes in the angle of incidence θ. In experiments performed at neutron spallation facilities, changes in the magnitude of the Q_z vector are obtained by both λ and θ variation. In these cases, λ is measured by the time-of-flight method (ToF). If not otherwise noted, NR measurements presented in this paper were performed at the Surface Profile Analysis Reflectometer beam line [Fig. 1(a)] at the Los Alamos Lujan Neutron Scattering Center.[52] The neutron beam is produced from a spallation source and moderated by liquid H_2. The different λ are discriminated by a ToF position-sensitive detector. The range of λ utilized in this work was from 4.5 to 16 Å. The reflectivity data are plotted as $R/R_{Fresnel}$ versus the perpendicular scattering vector Q_z, thus accounting for the Q_z^{-4} decrease of the reflectivity due to Fresnel's law.[53]

Unlike x-rays, neutron scattering lengths (amplitudes indicating the strength of interactions of neutron with the atomic nucleus) can vary for different isotopes of the same element. Frequently the so called isotopic substitution is used to increase or decrease the neutron scattering contrast of the measured system and its components. For that reason hydrogenous materials are frequently measured in D_2O rich subphases or vice-versa.

Analysis of the specular reflectivity versus Q_z enables development of the scattering length density (SLD) distribution normal to the sample surface.[54] SLD is a function of chemical composition and density of the material. The SLD profile obtained from NR measurements provides structural information at a very high spatial resolution (<10 Å). Specifications of NR measurements and modeling of the data have been detailed elsewhere.[52,54] If not noted otherwise, modeling of the SLD distributions was performed using an open-source reflectivity package, MOTOFIT, which runs in the IGOR Pro environment.[55] MOTOFIT approximates the continuous SLD function by a number of layers with constant SLDs. An error function centered between two adjacent interfaces is used to address the interfacial roughness. A theoretical reflectometry curve can be calculated using Abeles matrix formalism. Both Genetic optimization and Levenberg–Marquardt nonlinear least-square methods were employed to obtain the best fits with the lowest χ^2 values and structurally meaningful parameters for the NR data. To model the NR data, the SLD value of the quartz substrate was fixed at 4.18×10^{-6} Å^{-2} in all cases.

To illustrate the changes detectable by an NR experiment, simulated SLD distributions and corresponding calculated NR spectra are shown in Fig. 2. If any component of the system changes, e.g., the packing density of a lipid bilayer, the scattering length density distribution will change and will be immediately apparent in the neutron scattering. For example,

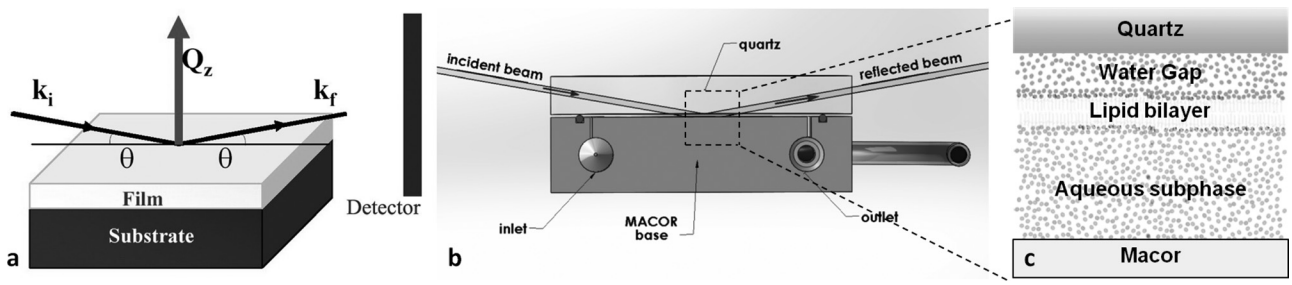

FIG. 1. Schematic of NR and solid–liquid interface flow cell. (a) Diagram of specular NR. The momentum transfer perpendicular to the interface, Q_z, given by the change in the incoming wave vector (k_i) and outgoing wavevector (k_f) on reflection at the boundary (k_f). (b) Side view of the flow cell used for the experiments. (c) Schematic of a lipid bilayer on a quartz wafer. (Not drawn to scale.) After deposition of the lipid bilayer, the quartz substrate was clamped against a Macor disk with a 0.1–0.3 mm thick, subphase-filled gap created by an O-ring. The neutron beam penetrated the lateral face of the quartz substrate and was scattered from the solid–liquid interface.

a rearrangement in the density or chemical composition of the bilayer, e.g., upon shear, can be observed as a change in the reflectivity signal. A modification of the thickness of the bilayer would result in altered fringe spacings. This is illustrated in Figs. 2(a) and 2(b) where the density, hydration, and interfacial roughness of all components were kept constant while the thickness of the lipid bilayer was varied. Figures 2(c) and 2(d) represent another case where the thickness and interfacial roughness of all the scattering components was kept constant but the amount of lipids in the bilayer, and hence the surface coverage, was decreased. This case would be visible as an increase of the SLD due to replacement of the regions not covered by the bilayer by the D_2O subphase.

We will discuss several cases of the NR experiments starting from the most simple and ending with the most complex systems.

III. RESULTS

A. Simple systems

NR is frequently executed to evaluate film thickness, roughness, packing, and chemical composition, but can also reveal the response of a (multi-)layer to external stimuli such as UV light,[56] shear,[46,57,58] electric fields,[59–61] change in temperature,[38,62,63] hydration,[38,64,65] or *p*H.[66–68]

In the following text, we will briefly discuss a few recent exemplary studies of our group, illustrating the potential and broadness of neutron reflectivity measurements for biorelated surfaces. The provided examples are by no means comprehensive and we invite the interested reader to study the above mentioned literature to gain a deeper understanding of the history and future potential of neutron reflectivity for the investigation of biorelated surfaces and interfaces.

1. Shear (stability of lipid bilayer)

Mechanical forces play a vital role in all living systems. For example, shear rates in the human body are in the order of $\sim 100\,s^{-1}$ in large veins to $\sim 1500\,s^{-1}$ in capillaries and arterioles.[69] In contrast, ocular shear rates range from 5000 to $28\,000\,s^{-1}$ based on the thickness of tear film of either 40 μm (Ref. 70) or 3 μm (Ref. 71) and a blink velocity of ~ 20 cm/s.[72] Hence, understanding the response of component properties of biological systems from lipid membranes to cell colonies and tissue to mechanical stress is of great importance in a variety of medical application.

In the human body, most interfaces are covered by lipid membranes and are exposed to flow, such as blood, air, bile, etc., and subsequent shear stress. Understanding how such thin films withstand these stimuli, and how their behavior deviates from tissue, has huge implications in many biomedical applications and problems.

To further our comprehension of such systems, we conducted several shear experiments in a custom-built neutron scattering solid–liquid interface flow cell (Fig. 3), similar to the ones that were presented by Hamiliton *et al.*[103] and Baker *et al.*[104] The measurement cell consists of two main parts: a base made of Macor ceramic [Fig. 3(a)] and a monocrystalline quartz wafer. The studied system (thin film, bilayer, living cells, etc.) is deposited on the bottom of the quartz disk [shown schematically in Fig. 3(b)]. The Macor part is equipped with a fluid inlet, outlet, and an O-ring

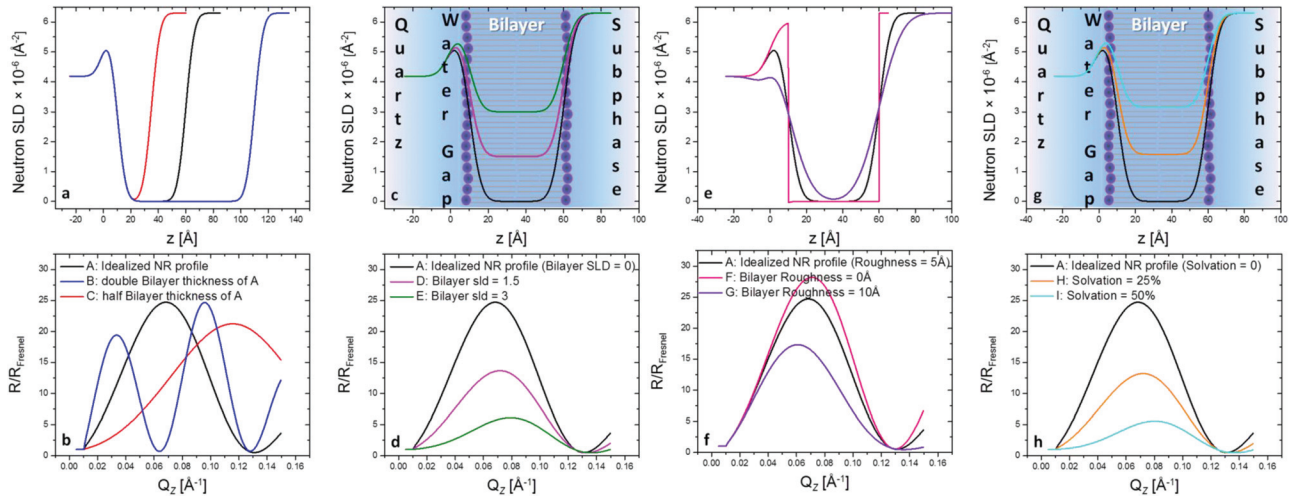

FIG. 2. Simulated SLD distributions and corresponding calculated NR spectra of a lipid bilayer in D_2O. Left panel (a)—three SLD distributions corresponding to the same (100% surface occupancy) density of the scattering components but with the thickness of the bilayer varied: 50, 100, and 25 Å. Right panel (b)—simulated Fresnel divided NR spectra corresponding to the SLD profiles shown in (a). (c) SLD distributions corresponding to the same thickness of the scattering components but with the SLD of the bilayer varied, simulating its different surface coverages: 100%, 75%, and 50%. (d) Calculated NR spectra corresponding to the SLD profiles shown in (c). (e) SLD distributions corresponding to the same thickness and SLD of the scattering components but with the roughness of the bilayer varied, simulating an undulating layer. (f) Calculated NR spectra corresponding to the SLD profiles shown in (e). (g) SLD distributions corresponding to the same thickness and SLD of the scattering components but with the solvation of the bilayer varied, simulating the effect of solvent penetration of 0%, 25%, and 50%. This has the same impact as changing the surface coverage shown in (c) and (d). (h) Calculated NR spectra corresponding to the SLD profiles shown in (g). For simplicity, in all cases the scattering contribution of the bilayer headgroups has been neglected and except for (e) and (d) the roughness parameter for all interfaces was set to 5 Å.

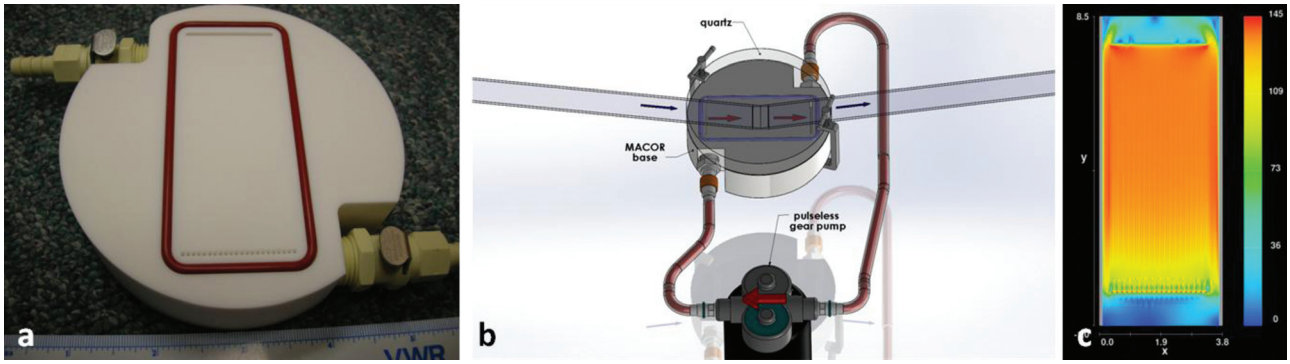

FIG. 3. Neutron scattering solid–liquid interface flow cell. (a) Picture of Macor flow cell base. (b) Schematic of the solid–liquid cell with clamping mechanism and pulse-less gear pump. (c) Results of hydrodynamic simulations of the fluid velocity distribution in the flow cell close to the quartz block, at the approximate location of the investigated systems.

groove. The O-ring separates the ceramic base from the quartz crystal. Both parts are kept together by a clamping mechanism. The distance between the ceramic base and the crystal is approximately 0.2 mm and can be regulated by the tension on the clamping system. The geometry of the measurement cell's inlets and outlets are designed to allow a laminar flow of liquid between the ceramic and the quartz. The laminarity of the flow was modeled by hydrodynamic simulations using commercial software [Fig. 3(c)] based on Navier–Stokes equations. The width and the length of the measurement cell over which the flow can be considered laminar is $35 \times 50\,\text{mm}^2$ and coincides with the size of the footprint of the neutron beam. A pulse-less gear pump was used to produce the flow required for the experiments.

At first, we investigated a bilayer made of zwitterionic 1,2-dipalmitoyl-sn-glycero-3-phosphoethanolamine (DPPE, transition temperature 63 °C), which is one of the phospholipids occurring in biological membranes,[73] under various shear stresses. The lipid bilayer was deposited by the Langmuir–Blodgett/Langmuir–Schäfer (LB/LS)[74,75] method directly on a monocrystalline quartz surface and investigated using NR in the above described solid–liquid interface flow cell. This cell allowed exercising a mechanical stress on the bilayer through a laminar flow of liquid parallel to the interface. Figure 4 shows the shear stress results. In the presented case, the shear rate was $55\,000\,\text{s}^{-1}$ exceeding the shear stress in a typical human capillary system by almost one and a half orders of magnitude. Even at a high shear rate or after changing the *p*H to very nonphysiological conditions, we could not observe a significant loss or rearrangement of the well-packed lipids during the shear stress experiments. This is important for the design of biomedical implants such as stents and grafts or other *in situ* applications because under conditions of high flow, particularly in the ascending aorta, the laminar flow of the blood can be disrupted and become turbulent. The above measurements offer a simplified description of the resistance of lipid bilayers to shear stress when deposited directly on a flat surface of the substrate. This not only gives interesting insights in the mode of action of our body but also offers implications for the design of biocompatible, functional coatings.

2. pH response of DPPE in phosphate buffered saline buffer

Thin polyelectrolyte multilayer (PEM) films deposited by layer-by-layer self-assembly technique[76–79] are being employed for a wide variety of applications such as targeted drug delivery, water desalination, and biosensors.[80–82] We fabricated lipid bilayers by LB/LS transfer deposited on PEM cushions.[83] Using NR, we discovered that the separation between a lipid bilayer and a PEM-covered substrate can be influenced by changing the *p*H of the aqueous

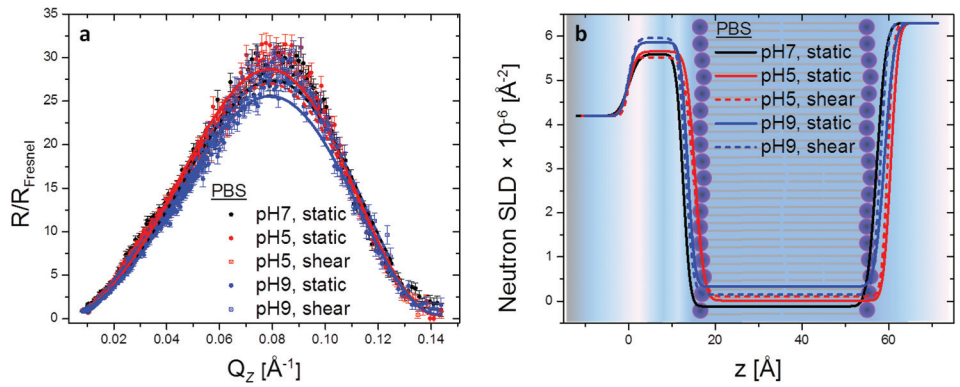

FIG. 4. DPPE bilayer at various *p*H show no adverse effect of high shear rates. (a) Fresnel normalized neutron reflectivity (R/R_F) of DPPE measured in static and shear ($55\,000\,\text{s}^{-1}$) conditions in phosphate buffered saline (PBS-D_2O) subphase at various *p*H and (b) the SLD profiles corresponding to the fits.

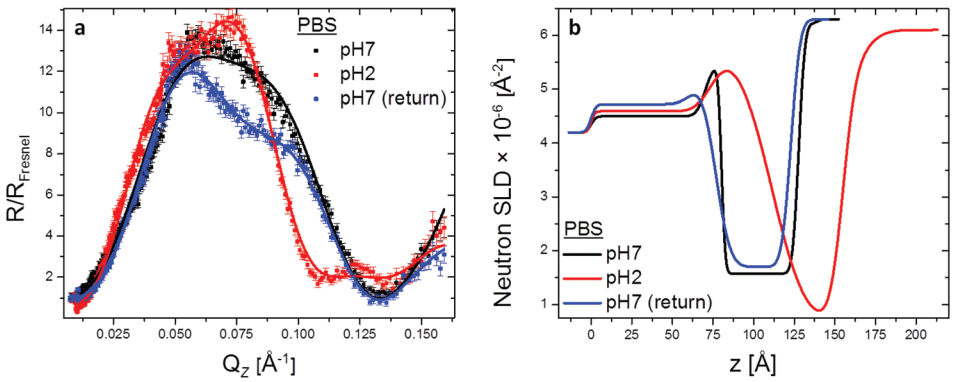

FIG. 5. Lipid bilayers deposited on PEM exhibited increased undulation in acidic environment. (a) Fresnel-divided NR measurements and corresponding SLD profiles, obtained from the fits, (b) of DPPC bilayer deposited on PEM ([PEI-PSS]$_3$-PEI). Measurements were performed in PBS at *p*H 7.0, *p*H 2.0, and *p*H again restored to 7.0. The error bars denote the standard deviation (SD) for each measurement.

environment. Decreasing the *p*H of the surrounding pure water subphase, and therefore changing the electrical properties of the system, significantly increases the distance between the lipid bilayer and the polyelectrolyte cushion due to electrostatic repulsion. Returning to the original *p*H reconstitutes the initial separation, with little or no change in the lipid bilayer structure. Hence, we are able to create a free floating lipid bilayer that is easy to attach and release to a substrate in a reversible manner. We hypothesize that this behavior is due to electrostatic repulsion between the lipid head groups and the polymer that increases when the *p*H is decreased.[67]

Below we present a case where the pure water subphase is replaced by PBS and a bilayer composed of 1,2-dipalmitoyl-sn-glycero-3-phosphocholine (DPPC, transition temperature 41 °C) molecules is used. Unlike the case of the pure water subphase, the use of PBS partially screens the charges on the lipids and polymers. As can be seen in Fig. 5, where the *p*H is decreased to *p*H 2, and the charge of the PEM changes from a net positive charge (*p*H 7) to a neutral PEM charge (*p*H 2), the bilayer interactions with the polymeric cushion weakens and the membrane starts to undulate. However, due to diminished electrostatic repulsion, no complete bilayer detachment was observed. The ability of the bilayer to decouple from the supporting layer, to undulate, and to induce curvature can be very beneficial for incorporating proteins or channels in the system, as the local curvature parameter is known to be crucial for interactions between a lipid bilayer and membrane proteins.[84] Moreover, such a free-floating bilayer, even if only partially removed from the underlying substrate, would be a more accurate platform for *in situ* studies of a variety of phenomena. Examples include flip-flop of membrane components, incorporation of transmembrane channels or interactions between a lipid bilayer and soluble proteins, interaction between membrane receptors and proteins, etc. Because most studied supported lipid bilayers tend to restrict the curvatures and motion of model membranes, this could result in decreased functionalities and lead to denaturation of the transmembrane proteins embedded in their structure. It needs to be stated that most biological systems only function well within a narrow *p*H range and changing it drastically might affect their viability. The authors are currently exploring the possibility of inducing the same repulsion by applying a small electric field, which would circumvent the drawbacks of an acidic environment.

B. Investigation of tethered lipid membranes under applied electric fields

In this example, polarized NR and a magnetic reference layer were employed to study structural changes in tethered lipid membranes induced by an electric potential applied across the bilayer. A tethered lipid membrane typically consists of hydrophilic polymers with functionalized ends such that one end binds to a substrate and the other incorporates within a lipid bilayer thereby "tethering" it to the surface.[85] Advantages of such architectures include (1) a planar membrane geometry enabling the application of surface sensitive techniques and use in biomimetic devices and (2) providing a highly hydrated cushion between membrane and support enabling fluctuations and facilitating the incorporation of transmembrane proteins into the bilayer.

Here, tethered lipid membranes were prepared on large surface area supports suitable for NR experiments using bifunctionalized polyethylene glycol (PEG) tethering molecules and primarily tail deuterated phospholipids. Sputter deposited Au thin films were coated on single crystal Si blocks (5.0 × 8.0 × 1.5 cm) to provide an electrode surface. A soft magnetic alloy, permalloy (Ni:Fe 4:1), was used as a binding layer between the gold and silicon. The permalloy also acted as a magnetic contrast layer, with a different magnetic SLD component depending on the spin direction of the atoms in the layer relative to the spin eigenstate of the incoming neutrons. Bifunctionalized PEG molecules ($n = 114$) with thiol and 1,2-distearoyl-*sn*-glycero-3-phosphoethanolamine (transition temperature 74 °C) terminal ends were obtained from Nanocs, Inc. (New York, NY) and used as tethering molecules on these solid supports. Dissolved in ethanol at a concentration of 1 mg/ml, the tethering molecule solution was incubated with the substrate for 5 h to form Au-thiol bonds

and yield a robust tethered layer. Subsequently, LB/LS deposition of phospholipids was employed to fill in remaining lipids and construct near complete coverage tethered lipid bilayer architectures. This method allowed for precise control of the constituent lipids of the membrane. For this work, tethered membranes were formed from either tail deuterated 1,2-distearoyl-*sn*-glycero-3-phosphocholine (DSPC, transition temperature 55 °C) or 8:2 M ratios of deuterated DSPC and protonated 1,2-dioctadecanoyl-sn-glycero-3-phosphoglycerol (DSPG, transition temperature 55 °C) obtained from Avanti Polar Lipids (Alabaster, AL). Samples were assembled within a solid–liquid interface flow cell containing protonated PBS and the capability of applying an electric potential between the Au surface (working electrode) and a Pt mesh (counter electrode) located 1 cm from the interface. High neutron scattering contrast between the deuterated lipids and the protonated solution and PEG tethers facilitated the precise localization and structural characterization of the membrane. Polarized NR experiments were performed on the POLREF instrument at ISIS, Oxfordshire, UK, with the sample placed in a fixed magnetic field such that the permalloy was saturated and its magnetic moment aligned either parallel or antiparallel to the incident neutron beam. Using up-stream spin flippers to alternate the incoming neutron polarization, the structure of the tethered membranes as a function of lipid composition and applied electric potential was monitored against two different contrasts of the permalloy layer without any disruption to the chemical or electrochemical state of the PEG or lipid layers.

For membranes composed only of DSPC, a zwitterionic lipid, a tethered membrane conformation with a highly hydrated space between the Au support and the bilayer was observed (data not shown) but no structural changes were detected as a function of electric potential. Of much greater interest were the results when anionic lipids (DSPG) were included in the membrane. In the 8:2 DSPC:DSPG case, measurements were performed over the following series of voltages: 0.0, +0.1, −0.1, 0.0, +0.5, −0.5, 0.0, +1.0, −1.0, +3.0, and +5.0 V. This series provided the ability to investigate the impacts of electric field polarity and magnitude on the charged, tethered membrane as well as the reversibility of the effects. The use of a magnetic reference layer and polarized NR allowed the simultaneous collection of two different neutron contrast scenarios without the necessity of solvent exchanges [Fig. 6(a)]. The collection of two SLD contrast conditions (only changing the magnetic polarization of the permalloy layer) allowed them to be simultaneously fit to minimize the uncertainty of the structural parameters. Using the RASCAL software package,[86] the measurements for all voltage conditions and the two polarization states were corefined to yield SLD distributions consistent with a native silicon oxide, the two metallic films, the hydrated cushion region, and the tethered membrane [Fig. 6(b)]. The observed SLD of the two spin states of the permalloy support was found to be similar to that described in previous polarized NR studies.[87] For simplicity, the tethered membrane SLD profiles for a subset of the measured voltage conditions are presented in Fig. 6(c). Due to the extremely high hydration of the PEG cushion region, the SLD of the cushion region could be fixed to that of PBS. Parameters corresponding to the bilayer region indicate a 44.4 ± 6.3 Å thickness, consistent with gel phase DSPC and DSPG bilayers, with 89.3% ± 3.8% coverage. For measurements over the series of applied fields, only the separation between the bilayer and the underlying support was allowed to vary. Our results clearly demonstrate that the spacing between the tethered bilayer and the support decreases with the application of a positive electric potential. At 0.0 V, the bilayer was separated from the Au surface by 43.8 ± 3.6 Å. This decreased to 33.7 ± 3.5 Å with the application of +1.0 V and to 20.3 ± 3.6 Å at a potential of +3.0 V. Increasing to +5.0 V did not result in any further decrease indicating that the tethering molecules were fully compressed. Further, for intermediate measurements at 0.0 V, the bilayer returned to its original position demonstrating the reversibility of the tether compression. Interestingly, the application of negative electric potentials did not increase the separation between the negatively charged bilayer and support.

This initial study demonstrates the electrochemical compression of surface-grafted polymers using charged lipid bilayers and the power of polarized NR for investigating soft matter samples. Understanding the forces acting on macromolecular structures at surfaces is vital to a number of different branches of science and engineering, ranging from biofouling to surface lubrication. A variety of experimental techniques have been developed to study these forces directly, including a lot of pioneering work using surface force apparatus[88] and AFM.[89] Here, we demonstrate a potential next step for the analysis of surface forces and their structural implications, using the semipermeable nature of charged lipid membranes to directly compress surface bound polymer layers as a function of the applied electrical potential.

C. Off-specular studies on in-plane correlations in lipid membranes

Another application of neutron surface scattering techniques is to provide information about fluctuations or lateral structures with length scales on the order of microns along the surface of the studied system using the off-specular (or diffuse) scattering signal which, using a position sensitive detector, can be recorded simultaneously with NR. Distorted wave born approximation (DWBA) theory states that the intensity distribution of the off-specular scattering ($p_i - p_f \neq 0$) directly corresponds to the degree of interfacial fluctuations.[90,91] A two-dimensional intensity map as a function of p_i ($p_i = 2\pi \sin \alpha_i/\lambda$) and p_f ($p_f = 2\pi \sin \alpha_f/\lambda$), where α_i and α_f are the angles of the incoming and outgoing neutrons, respectively, and λ is the wavelength of the neutrons, clearly highlights the dominating intensity peak at $p_i - p_f = 0$ corresponding to the specular reflection, but also allows for the visualization of the off-specular scattering.[92] The latter indicates the presence of surface and substrate roughness and nicely showcases any developments in in-plane fluctuations due to changing experimental conditions.

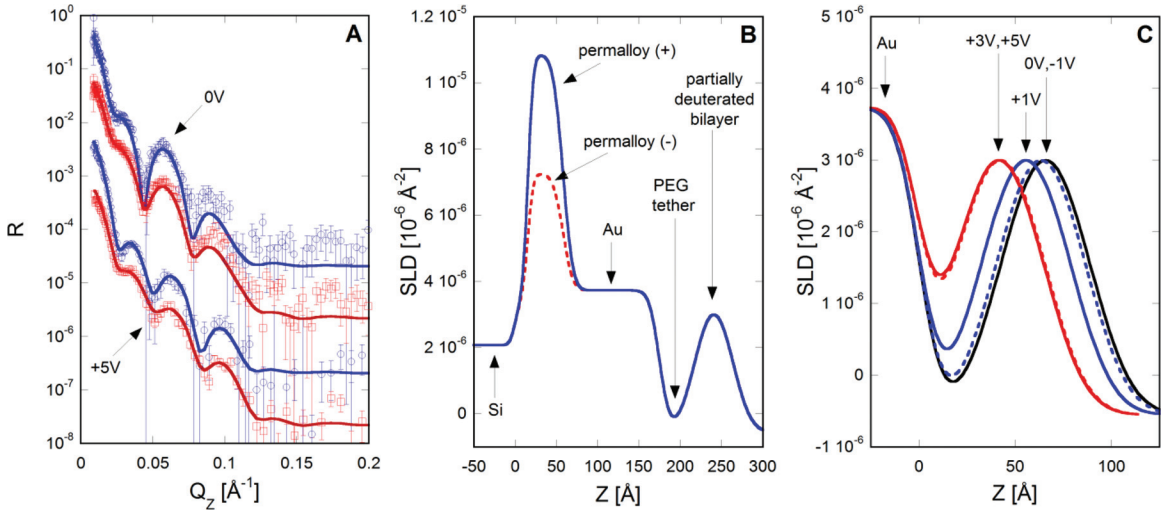

FIG. 6. Polarized NR measurements of the structure of a tethered bilayer composed of 8:2 DSPC:DSPG exposed to applied electric fields. Panel (a) displays representative NR data and fits for the 0.0 V (top) and +5.0 V (bottom) cases. Spin up data (+) are shown in blue and spin down (–) in red. Data are shifted vertically for clarity. The full SLD profiles of the 0.0 V case in panel (b) show the different magnetic scattering lengths of the two spin states in the permalloy magnetic contrast layer. Zooming in on the tethered bilayer region [panel (c)] demonstrates that the application of positive electric potentials compresses the tethering polymer and decreases the spacing between the substrate and bilayer.

As one example, we studied poly(*N*-isopropylacrylamide) (pNIPAAm)-supported single lipid bilayers,[90] which can serve as models of cell membranes. By permitting the structural freedom of the membrane, they more accurately reproduce cellular membrane morphology compared to directly supported bilayers. Moreover, they also allow for the incorporation of membrane-bound proteins while potentially minimizing their denaturation.

By modeling the off-specular scattering, we were able to quantify in-plane height-height correlations of interfacial fluctuations of a DPPC bilayer supported on pNIPAAm as a function of temperature. As the temperature decreased from 37 to 25 °C, the polymer swelled and the supported lipid membrane deviated from its initially nearly planar structure. Further analysis of the data revealed that correlation lengths characteristic of capillary waves changed from 30 μm at 37 °C to 11 μm at 25 °C, while the membrane bending rigidity remains roughly constant in this temperature range.

Analysis of the off-specular scattering can provide a powerful tool for understanding the complex behavior of cellular membranes, protein transport and docking, lipid segregation into ordered domains, and modification of bulk membrane elastic properties due to membrane constituents and external stimuli. By successfully mimicking the complexity of cellular membrane morphology, the presented polymer-membrane system opens the door for numerous other investigative opportunities in the future, e.g., how biological agents such as toxins, viruses, and other pathogens affect in- and out-of-plane membrane structures.

D. Study of adhesion of living cells to the solid substrate

In a significant advancement toward employing neutron reflectometry to measure complex biological samples, we studied live cells adhered to a quartz substrate.[47] Neutrons are the perfect probe for the investigation of living tissue because they offer unparalleled resolution on the 1–1000 Å level where even the best microscopy techniques fail. Moreover, NR provides global information about the cellular monolayer averaged over the footprint size. Lastly, neutrons are ideal for working with living systems such as cells because, unlike x-rays, they have a nonperturbative nature. In a series of preliminary experiments, we showed that NR is capable of probing the composition and thickness of the interfacial area between the lipid plasma membrane and the rigid substrate.

Measurements were conducted on live cell monolayers grown on a flat surface of monocrystalline quartz. Cell monolayers were perfused with culture medium at controlled conditions to reach a laminar shear stress level of 1.5 Pa or left static, as previously described.[47]

In all experimental data presented below, D_2O based buffers were used as the subphase. From our experience, we know that the cells can survive up to 6 h in such conditions without visible changes in the cells' viability. Using D_2O based subphases was necessary to obtain sufficient scattering contrast. The main source of such contrast is due to the neutron scattering differences between the hydrogenated lipid membrane (low SLD) facing the quartz substrate and the D_2O environment (high SLDs).

In a series of experiments, we observed a clear signal attributable to live HK-03 mouse fibroblast cells, as confirmed by comparison with samples of pure medium. We believe these experiments represent the first successful visualization and quantization of the interface between live cells and a substrate using NR. Due to the pronounced neutron scattering from the hydrogenated alkyl tails of the phospholipid bilayers (which are not capable of an isotopic exchange), we were able to clearly distinguish the lipid membrane of the

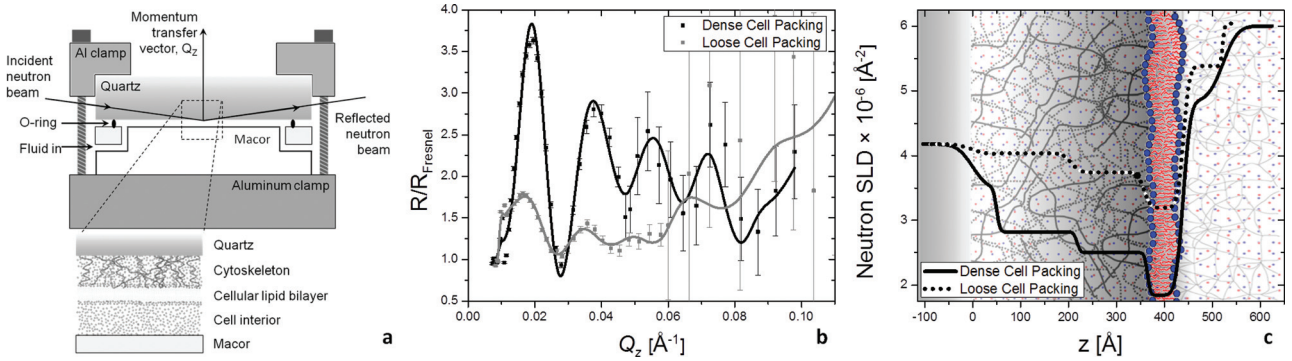

FIG. 7. Schematic of solid–liquid interface flow cell used for all live cell experiments + NR profiles and corresponding SLD distributions of mouse fibroblasts (a). Schematic representation of the neutron measurement cell used. Confluent layer of cells is grown on the quartz substrate that is inverted into the measurement cell. A neutron beam enters through the quartz at a glancing angle and scatters from the adhesion layer and cell membrane interfaces. Fresnel divided NR profiles (b) and corresponding SLD profiles (c) for high (black) and low (gray) cell surface densities. NR data are shown by closed squares, and error bars indicate 1 SD. The lower surface cell density is evident from the decreased scattering intensity (b) and the increased SLD in the membrane region (360–440 Å) and interior of the cell (440–600 Å) (b).

live cells from the deuterated environment. With an approx. 80 Å thickness (Fig. 7), the membrane region was measured to be twice as thick as the length of two hydrophobic tails, indicating that the adhering cells were not organized as a homogeneous plane uniformly spaced on the quartz substrate. This suggests that the membrane is either undulating, nonhomogeneously distributed due to the surface topography of the underlying media and adherence proteins, or that the scattered neutron, averaged over several neighboring cells, varied in their distance from the solid substrate.

Those very simplistic experiments visualizing the adherence layer of mouse fibroblasts to a quartz substrate show how powerful NR is, compared to other surface techniques such as AFM and various microscopies, for unraveling the information about buried subphases. In the last paragraph, we would like to go one step further and present in detail a much more complex and medically relevant system.

E. Investigation of off-specular scattering of endothelial adhesion at varying temperatures and fluid shear stress

As mentioned above, mechanical forces play an intricate role in biological systems from the tissue and organ level down to individual cells and proteins.[93–95] Certain tissues are inherently reliant on solid mechanical and fluid mechanical stresses for normal healthy function. The foremost among these is the vascular system encompassing all blood vessels.[95] The innermost layer of blood vessels, which makes contact with blood, is composed of a single monolayer of endothelial cells. Endothelial cells are the main gatekeepers of a key function of blood vessels known as vascular permeability. Blood vessels must strike a delicate balance in allowing fluid and cellular flux across their wall. In healthy people, vascular permeability (degree of transblood vessel flux) is tightly controlled, however in certain diseases it becomes deranged with devastating consequences. Among these diseases is acute respiratory distress syndrome (ARDS). In ARDS, the blood vessels located in our lungs become extremely leaky leading to pulmonary edema, i.e., accumulation of fluid in the lungs that severely curtails the lung's oxygen diffusion capacity. It is believed that mechanical stress in the form of both cyclic elastic stress and fluid shear stress from blood flow are key components in regulating endothelial permeability and play roles in diseases such as ARDS.[96,97]

Adhesion to the underlying extracellular matrix (ECM) is a crucial component of how endothelial cells sense and transmit mechanical signals. NR was used for the first time to measure the nanoscopic structure of the adhesion layer of confluent endothelial cells.[46] As in the case discussed above, neutron scattering is probing only the interfacial space between the lipid plasma membrane and the rigid substrate. Endothelial cells generate their own extracellular matrix (basal lamina) making it possible to grow monolayers on inert surfaces like quartz without prior exogenous deposition of protein layers.[98,99] We grew confluent monolayers of human pulmonary arterial endothelial cells on single quartz blocks. They were then subjected to NR under shear stress of $\tau = 1.5$ Pa (equivalent to arterial conditions).

We observed that the basal lamina thickness l is highly sensitive to changes in temperature or shear stress.

Under static conditions [Figs. 8(b) and 8(c)], we observed a near tripling of l as the temperature was raised from 25 to 37 °C ($l^{st}_{25\,°C} \approx 200$ Å, $l^{st}_{37\,°C} \approx 600$ Å). Interestingly, shear stress has the opposite effect at the two temperatures [Figs. 8(d) and 8(e)], causing cell separation at 25 °C while inducing movement closer to the substrate at physiologic temperature ($l^{ss}_{25\,°C} \approx 700$ Å, $l^{ss}_{37\,°C} \approx 200$ Å).

We also analyzed the off-specular scattering since the scattered neutron intensity as a function of the in-plane components of the momentum transfer vector provides valuable information about fluctuations along the surface of the cell monolayer. Figure 9 shows the off-specular neutron reflectivity data at 25 °C. The high intensity peak at $p_i - p_f = 0$ corresponds to the specular reflection. DWBA states that the intensity distribution of the off-specular scattering ($p_i - p_f \neq 0$) directly corresponds to the degree of interfacial

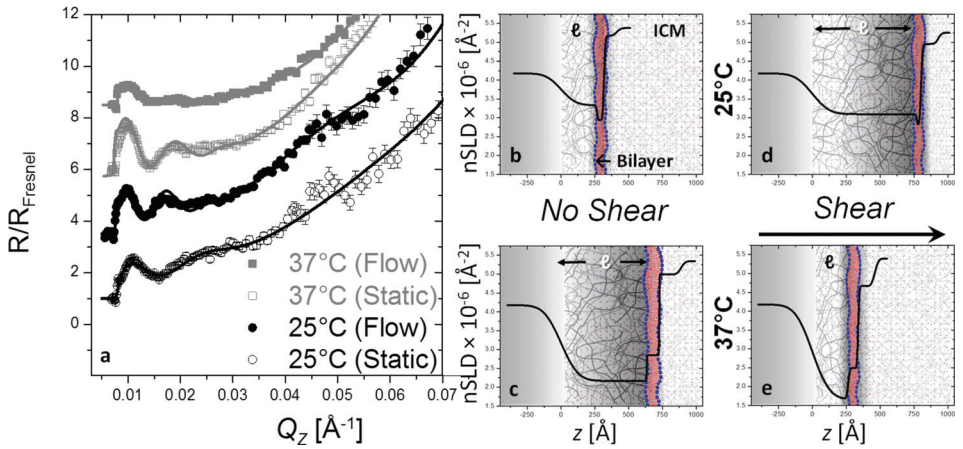

FIG. 8. Differences in response to shear flow of healthy endothelial cells at ambient and physiological temperatures. Left (a) Fresnel-divided NR measurements (circles/squares with error bars) and corresponding best-fit models (solid lines) at the conditions studied. Black (open circles): 25° (static), black (closed circles): 25° (shear), gray (open squares): 37° (static), gray (closed squares): 37° (shear). The NR spectra are offset along y-axis for clarity. Right [(b)–(e)]: SLD profiles obtained by fitting the data sets using a 3-box model (extracellular matrix—cell membrane—partial cell interior).

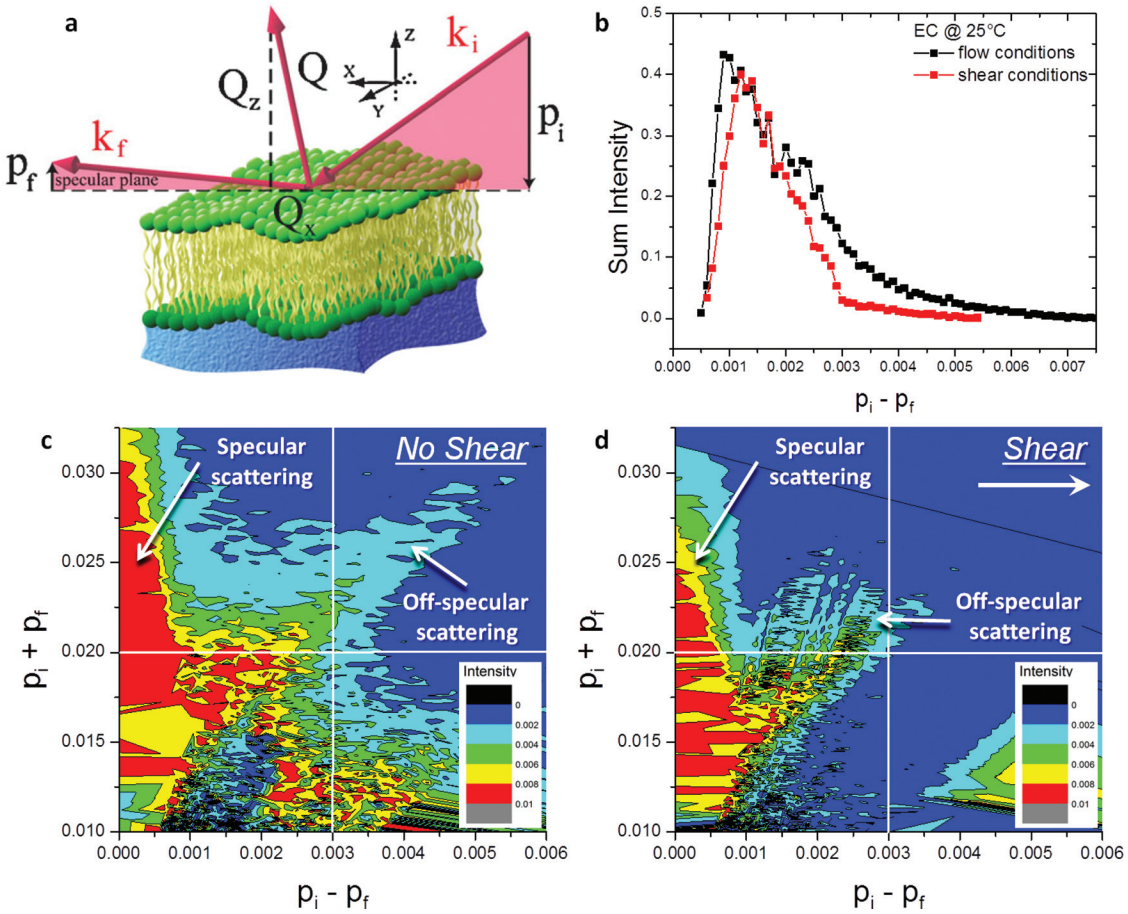

FIG. 9. Off-specular data depicts changes in surface roughness at 25 °C: Data is shown as two-dimensional intensity maps as a function of p_i and p_f. (a) $p_i = 2\pi \sin \alpha_i/\lambda$ and $p_f = 2\pi \sin \alpha_f/\lambda$ are the components perpendicular to the sample surface of the incoming and outgoing neutron wave vectors, respectively (Ref. 92). The dominating intensity peak at $p_i - p_f = 0$ corresponds to the specular reflection. The off-specular is visible to the right from the specular line along picture's diagonal indicating the presence of surface and substrate roughness. (b) Comparison of the intensity distribution along the peaks vs $p_i - p_f$ of endothelial cells under static (black) and shear (red) conditions show decrease in scattering under shear stress. (c) and (d) show experimental two-dimensional intensity maps of endothelial cells at 37 °C at static and shear conditions, respectively. The extension of the off-specular signal (right top corner) in (c) compared to (d) indicates more in-plane fluctuations at static conditions.

fluctuations.[90] Our data show that the off-specular peak enlarges with increasing temperature under static conditions (data for 37 °C not shown) while it substantially decreases with shear flow for both temperatures. Temperature, as expected, increases interfacial thermal fluctuations. Shear stress acts in a reverse manner by placing the cells (and therefore their lipid membranes) under tension, thereby suppressing fluctuations and decreasing the off-specular intensity.

From individual cells and proteins up to complete tissue and organs, mechanical forces play an intricate role in biological systems.[93–95] Due to the limitation of most techniques, the existing work in mechanobiology has focused on cells, single molecules, and protein complexes, leaving the collective behavior of cell monolayers less well explored.

The strength of neutron reflectometry is its nonperturbative nature, the ability to probe large surface areas of buried interfaces with nanometer resolution, and the possibility of scattering contrast manipulation via the isotopic substitutions. That allows us to probe details of the cell–substrate interface that are not accessible with any other standard techniques. Such capabilities can also be employed to obtain better insight into the mechanisms of cell adhesion and cell–surface properties of clinically relevant systems. For example, the above results demonstrate that neutron reflectometry experiments can provide valuable insight into complex biomedical systems, such as living human cells under fluid mechanical shear stress. Specifically, the above studies could show the major redistribution of proteins involved in cell–cell and cell–substrate adhesion shear stress is causing, even on relatively short biological time scales (4 h) relevant to the time scale of our neutron experiments. The localization of adhesion proteins is postulated to promote linkage between the actin skeleton and extracellular matrix, forming enhanced adhesion zones.[96] Shear stress at 37 °C caused localization of specific proteins, which may alter the adhesion potential in favor of overall increased adhesion as measured with neutrons. This biological response competes against the purely physical effects of shear flow observed at 25 °C and the increased repulsive potential of the basal lamina at higher temperatures. Those findings may lead to advances in the treatment of atherosclerosis and other disorders associated with the cardiovascular system, but also open the door to a complete new way of investigating and understanding living tissue *in-situ*.

In this spirit, we have started to expand those studies to glioblastoma (GBM),[45] one of the most common and aggressive type of brain tumors.[100] Under static conditions, we have observed profound differences in noninvasive U251 cells, compared to the invasive CNS1 and GL261 cells. Namely, the human U251 cells showed a much thicker glycocalyx or "adhesion" layer than the cells derived from rat and mouse. We hypothesized that U251 cells may have a higher production of hyaluronic acid (HA) and associated proteoglycans[101] than the rodent GBM cells. This could contribute both to the nonfibroblastic morphology and limited invasive ability since a thick HA coating can promote cell adhesion, but limit GBM invasion *in vivo* if not degraded by tumor-produced hyaluronidases.[102] In summary, the presented results reveal differences in the thickness and composition of adhesion layers of different GBM cells in the static conditions as well as changes to this layer when the cells were subjected to shear stress. These differences may be specifically associated with mechanisms of brain tumor invasion. Further studies of these cells by neutron reflectometry under a variety of conditions (surface coatings, flow, and drug treatments) will allow to determine conditions triggering changes in the composition, density, and thickness of the biomaterial at the cell surface (in our case, the ECM layer). This, in turn, can help to identify changes that correlate with increased or decreased tumor invasiveness. Pursuit of those studies can have significant medical impact for the development of targeted anti-invasive therapies for GBM. Also, by revealing differences that may be specifically associated with mechanisms of brain tumor invasion, NR shows the power it holds for understanding biomedical questions.

IV. CONCLUSION AND OUTLOOK

The discussed experiments illustrate the potential of NR in addressing the structural properties of soft materials from simple supported lipid membranes in static and dynamic conditions to the adherence of complex endothelial cells under liquid shear stress.

We hope that an inclined reader will utilize some of these concepts and experimental approaches to conduct new studies that will provide better understanding of biomedical questions, suggest innovative treatment, or advance the development of novel biomimetic materials.

ACKNOWLEDGMENTS

This work benefited from the use of the Lujan Neutron Scattering Center at Los Alamos Neutron Science Center funded by the DOE Office of Basic Energy Sciences and Los Alamos National Laboratory under DOE Contract No. DE-AC52-06NA25396. The authors thank the ISIS Neutron Source (STFC, UK) for access to neutron facilities on POLREF through Proposal No. RB1120119.

[1]J. Daillant and A. Gibaud, Lect. Notes Phys. **770**, 133 (2009).
[2]G. Fragneto-Cusani, J. Phys.: Condens. Matter **13**, 4973 (2001).
[3]J. Penfold, Curr. Opin. Colloid Interface Sci. **7**, 139 (2002).
[4]A. S. Curtis, J. Cell Biol. **20**, 199 (1964).
[5]D. Gingell and I. Todd, Biophys. J. **26**, 507 (1979).
[6]C. S. Izzard and L. R. Lochner, J. Cell Sci. **21**, 129 (1976).
[7]M. Schindl, E. Wallraff, B. Deubzer, W. Witke, G. Gerisch, and E. Sackmann, Biophys. J. **68**, 1177 (1995).
[8]H. Verschueren, J. Cell Sci. **75**, 279 (1985).
[9]D. Braun and P. Fromherz, Appl. Phys. A **65**, 341 (1997).
[10]D. Braun and P. Fromherz, Phys. Rev. Lett. **81**, 5241 (1998).
[11]R. Parthasarathy and J. T. Groves, Cell Biochem. Biophys. **41**, 391 (2004).
[12]D. Axelrod, J. Cell Biol. **89**, 141 (1981).
[13]J. S. Burmeister, L. A. Olivier, W. M. Reichert, and G. A. Truskey, Biomaterials **19**, 307 (1998).
[14]J. S. Burmeister, G. A. Truskey, and W. M. Reichert, J Microsc. **173**, 39 (1994).
[15]D. Gingell, I. Todd, and J. Bailey, J. Cell Biol. **100**, 1334 (1985).

[16]D. K. Hoover, E.-J. Lee, and M. N. Yousaf, Langmuir: ACS J. Surf. Colloids **25**, 2563 (2009).
[17]K. Giebel, C. Bechinger, S. Herminghaus, M. Riedel, P. Leiderer, U. Weiland, and M. Bastmeyer, Biophys. J. **76**, 509 (1999).
[18]A. W. Peterson, M. Halter, A. Tona, K. Bhadriraju, and A. L. Plant, BMC Cell Biol. **10**, 16 (2009).
[19]A. M. Butt, H. C. Jones, and N. J. Abbott, J. Physiol. **429**, 47 (1990).
[20]M. J. Rutten, R. L. Hoover, and M. J. Karnovsky, Brain Res. **425**, 301 (1987).
[21]P. A. Vogel, S. T. Halpin, R. S. Martin, and D. M. Spence, Anal. Chem. **83**, 4296 (2011).
[22]J. Wegener, M. Sieber, and H.-J. Galla, J. Biochem. Biophys. Methods **32**, 151 (1996).
[23]D. P. Allison, N. P. Mortensen, C. J. Sullivan, and M. J. Doktycz, Wiley Interdiscip. Rev.: Nanomed. Nanobiotechnol. **2**, 618 (2010).
[24]R. Lal and S. A. John, Am. J. Physiol.: Cell Physiol. **35**, 1 (1994).
[25]D. J. Müller and Y. F. Dufrêne, Trends Cell Biol. **21**, 461 (2011).
[26]A. Vinckier and G. Semenza, FEBS Lett. **430**, 12 (1998).
[27]K. Cheung, S. Gawad, and P. Renaud, Cytometry, Part A **65A**, 124 (2005).
[28]J. E. da Silva, J. P. M. de Sá, and J. Jossinet, Med. Biol. Eng. Comput. **38**, 26 (2000).
[29]D. A. Dean, T. Ramanathan, D. Machado, and R. Sundararajan, J. Electrost. **66**, 165 (2008).
[30]S. Krueger, Curr. Opin. Colloid Interface Sci. **6**, 111 (2001).
[31]J. Majewski, T. L. Kuhl, M. C. Gerstenberg, J. N. Israelachvili, and G. S. Smith, J. Phys. Chem. B **101**, 3122 (1997).
[32]I. Burgess, M. Li, S. L. Horswell, G. Szymanski, J. Lipkowski, J. Majewski, and S. Satija, Biophys. J. **86**, 1763 (2004).
[33]G. Fragneto, F. Graner, T. Charitat, P. Dubos, and E. Bellet-Amalric, Langmuir **16**, 4581 (2000).
[34]B. W. Koenig, S. Krueger, W. J. Orts, C. F. Majkrzak, N. F. Berk, J. V. Silverton, and K. Gawrisch, Langmuir **12**, 1343 (1996).
[35]S. Krueger, J. F. Ankner, S. K. Satija, C. F. Majkrzak, D. Gurley, and M. Colombini, Langmuir **11**, 3218 (1995).
[36]D. A. Doshi, A. M. Dattelbaum, E. B. Watkins, C. J. Brinker, B. I. Swanson, A. P. Shreve, A. N. Parikh, and J. Majewski, Langmuir: ACS J. Surf. Colloids **21**, 2865 (2005).
[37]A. Junghans and I. Köper, Langmuir **26**, 11035 (2010).
[38]H. L. Smith, M. S. Jablin, A. Vidyasagar, J. Saiz, E. Watkins, R. Toomey, A. J. Hurd, and J. Majewski, Phys. Rev. Lett. **102**, 228102 (2009).
[39]J. Fitter, T. Gutberlet, and J. Katsaras, *Neutron Scattering in Biology: Techniques and Applications* (Springer-Verlag, Berlin Heidelberg, 2006).
[40]G. Pabst, N. Kučerka, M. P. Nieh, M. C. Rheinstädter, and J. Katsaras, Chem. Phys. Lipids **163**, 460 (2010).
[41]J. Penfold and R. K. Thomas, Curr. Opin. Colloid Interface Sci. **19**, 198 (2014).
[42]H. P. Wacklin, Curr. Opin. Colloid Interface Sci. **15**, 445 (2010).
[43]C. J. Garvey, R. B. Knott, E. Drabarek, and P. W. Kuchel, Eur. Biophys. J. **33**, 589 (2004).
[44]A. M. Stadler, C. J. Garvey, A. Bocahut, S. Sacquin-Mora, I. Digel, G. J. Schneider, F. Natali, G. M. Artmann, and G. Zaccai, J. R. Soc. Interface **9**, 2845 (2012).
[45]A. Junghans, M. J. Waltman, H. L. Smith, L. Pocivavsek, N. Zebda, K. Birukov, M. Viapiano, and J. Majewski, Mod. Phys. Lett. B **28**, 1430015 (2014).
[46]L. Pocivavsek, A. Junghans, N. Zebda, K. Birukov, and J. Majewski, Am. J. Physiol.: Lung Cell. Mol. Physiol. **306**, L1 (2014).
[47]H. L. Smith, J. Hickey, M. S. Jablin, A. Trujillo, J. P. Freyer, and J. Majewski, Biophys. J. **98**, 793 (2010).
[48]P. S. Swain and D. Andelman, Langmuir **15**, 8902 (1999).
[49]J. Raedler, H. Strey, and E. Sackmann, Langmuir **11**, 4539 (1995).
[50]E. T. Castellana and P. S. Cremer, Surf. Sci. Rep. **61**, 429 (2006).
[51]E. Sackmann, Science **271**, 43 (1996).
[52]M. Dubey, M. S. Jablin, P. Wang, M. Mocko, and J. Majewski, Eur. Phys. J. Plus **126**, 110 (2011).
[53]J. Als-Nielsen, Phys. A: Stat. Mech. Appl. **140**, 376 (1986).
[54]J. Penfold and R. K. Thomas, J. Phys.: Condens. Matter **2**, 1369 (1990).
[55]A. Nelson, J. Appl. Crystallogr. **39**, 273 (2006).
[56]H. L. Smith, M. C. Howland, A. W. Szmodis, Q. Li, L. L. Daemen, A. N. Parikh, and J. Majewski, J. Am. Chem. Soc. **131**, 3631 (2009).
[57]S. M. Baker, G. S. Smith, D. L. Anastassopoulos, C. Toprakcioglu, A. A. Vradis, and D. G. Bucknall, Macromolecules **33**, 1120 (2000).
[58]J. Penfold, E. Staples, I. Tucker, and G. Fragnetto, Phys. B: Condens. Matter **221**, 325 (1996).
[59]I. Burgess, M. Li, S. L. Horswell, G. Szymanski, J. Lipkowski, S. Satija, and J. Majewski, Colloids Surf. B – Biointerfaces **40**, 117 (2005).
[60]S. Lecuyer, G. Fragneto, and T. Charitat, Eur. Phys. J. E: Soft Matter Biol. Phys. **21**, 153 (2006).
[61]P. Mansky, J. DeRouchey, T. P. Russell, J. Mays, M. Pitsikalis, T. Morkved, and H. Jaeger, Macromolecules **31**, 4399 (1998).
[62]W. J. Orts, J. H. van Zanten, W.-L. Wu, and S. K. Satija, Phys. Rev. Lett. **71**, 867 (1993).
[63]R. Steitz, V. Leiner, K. Tauer, V. Khrenov, and R. v. Klitzing, Appl. Phys. A **74**, s519 (2002).
[64]J. Generosi, C. Castellano, D. Pozzi, A. C. Castellano, R. Felici, F. Natali, and G. Fragneto, J. Appl. Phys. **96**, 6839 (2004).
[65]M. Lösche, J. Schmitt, G. Decher, W. G. Bouwman, and K. Kjaer, Macromolecules **31**, 8893 (1998).
[66]S. W. An, R. K. Thomas, F. L. Baines, N. C. Billingham, S. P. Armes, and J. Penfold, J. Phys. Chem. B **102**, 5120 (1998).
[67]S. Singh, A. Junghans, J. Tian, M. Dubey, S. Gnanakaran, J. Chlistunoff, and J. Majewski, Soft Matter **9**, 8938 (2013).
[68]T. J. Su, J. R. Lu, R. K. Thomas, Z. F. Cui, and J. Penfold, Langmuir **14**, 438 (1998).
[69]T. G. Papaioannou and C. Stefanadis, Hell. J. Cardiol. **46**, 9 (2005).
[70]J. I. Prydal, P. Artal, H. Woon, and F. W. Campbell, Invest. Ophthalmol. Visual Sci. **33**, 2006 (1992).
[71]P. E. King-Smith, B. A. Fink, N. Fogt, K. K. Nichols, R. M. Hill, and G. S. Wilson, Invest. Ophthalmol. Visual Sci. **41**, 3348 (2000).
[72]A. Heryudono, R. J. Braun, T. A. Driscoll, K. L. Maki, L. P. Cook, and P. E. King-Smith, Math. Med. Biol. **24**, 347 (2007).
[73]H. Lodish, A. Berk, S. L. Zipursky, P. Matsudaira, D. Baltimore, and J. Darnell, *Molecular Cell Biology*, 4th ed. (W. H. Freeman, San Francisco, 2000).
[74]I. Langmuir, J. Franklin Inst. **218**, 143 (1934).
[75]I. Langmuir and V. J. Schaefer, Chem. Rev. **24**, 181 (1939).
[76]R. K. Iler, J. Colloid Interface Sci. **21**, 569 (1966).
[77]G. Decher, Science **277**, 1232 (1997).
[78]J. Schmitt, T. Gruenewald, G. Decher, P. S. Pershan, K. Kjaer, and M. Loesche, Macromolecules **26**, 7058 (1993).
[79]H. Ai, S. Jones, and Y. Lvov, Cell Biochem. Biophys. **39**, 23 (2003).
[80]X. Liu and M. L. Bruening, Chem. Mater. **16**, 351 (2004).
[81]S. Singh and M. McShane, Biosens. Bioelctron. **25**, 1075 (2010).
[82]E. W. Stein, S. Singh, and M. J. McShane, Anal. Chem. **80**, 1408 (2008).
[83]S. Singh, A. Junghans, M. J. Waltman, A. Nagy, R. Iyer, and J. Majewski, Soft Matter **8**, 11484 (2012).
[84]H. T. McMahon and J. L. Gallop, Nature **438**, 590 (2005).
[85]E. B. Watkins, R. J. El-khouri, C. E. Miller, B. G. Seaby, J. Majewski, C. M. Marques, and T. L. Kuhl, Langmuir **27**, 13618 (2011).
[86]A. Hughes, RasCAL (2014), see http://sourceforge.net/projects/rscl/.
[87]S. A. Holt, A. P. Le Brun, C. F. Majkrzak, D. J. McGillivray, F. Heinrich, M. Lösche, and J. H. Lakey, Soft Matter **5**, 2576 (2009).
[88]J. N. Israelachvili, *Intermolecular and Surface Forces* (Academic, New York, 2011).
[89]J. F. Joanny, Interface Sci. **11**, 157 (2003).
[90]M. S. Jablin, M. Zhernenkov, B. P. Toperverg, M. Dubey, H. L. Smith, A. Vidyasagar, R. Toomey, A. J. Hurd, and J. Majewski, Phys. Rev. Lett. **106**, 138101 (2011).
[91]L. Gösta and W. L. Stephen, Phys. Scr. **53**, 734 (1996).
[92]V. Lauter-Pasyuk, H. J. Lauter, G. P. Gordeev, P. Müller-Buschbaum, B. P. Toperverg, M. Jernenkov, and W. Petry, Langmuir **19**, 7783 (2003).
[93]B. Alberts, D. Bray, J. Lewis, M. Ra, K. Roberts, and J. D. Watson, *Molecular Biology of the Cell* (Garland Publishing, New York, 1994).
[94]D. Boal, *Mechanics of the Cell* (Cambridge University, Cambridge, 2002).
[95]Y.-T. Shiu, "Mechanical forces on cells," in *The Biomedical Engineering Handbook: Tissue Engineering and Artificial Organs*, 3rd ed. (CRC Press Taylor & Francis Group, LLC, Boca Raton, FL, 2006), pp. 33.31–33.18.

[96]K. G. Birukov, A. A. Birukova, S. M. Dudek, A. D. Verin, M. T. Crow, X. Zhan, N. DePaola, and J. G. N. Garcia, Am. J. Respir. Cell Mol. Biol. **26**, 453 (2002).
[97]A. A. Birukova, S. Chatchavalvanich, A. Rios, K. Kawkitinarong, J. G. N. Garcia, and K. G. Birukov, Am. J. Pathol. **168**, 1749 (2006).
[98]K. G. Birukov, N. Leitinger, V. N. Bochkov, and J. G. N. Garcia, Microvas. Res. **67**, 18 (2004).
[99]B. V. Howard, E. J. Macarak, D. Gunson, and N. A. Kefalides, Proc. Natl. Acad. Sci. U. S. A. **73**, 2361 (1976).
[100]D. N. Louis, Annu. Rev. Pathol.: Mech. Dis. **1**, 97 (2006).
[101]M. S. Viapiano and S. E. Lawler, *CNS Cancer: Models, Prognostic Factors and Targets*, edited by E. Van Meir (Humana, NJ, 2009), pp. 1219–1252.
[102]B. Enegd, J. A. King, S. Stylli, L. Paradiso, A. H. Kaye, and U. Novak, Neurosurgery **50**, 1311 (2002).
[103]W. A. Hamilton, P. D. Butler, S. M. Baker, G. S. Smith, J. B. Hayter, L. J. Magid, and R. Pynn, Phys. Rev. Lett. **72**, 2219 (1994).
[104]S. M. Baker, P. D. Butler, W. A. Hamilton, J. B. Hayter, and G. S. Smith, Rev. Sci. Instrum. **65**, 412 (1994).